Thermal effects on a passive wireless antenna sensor for strain and crack sensing

Xiaohua Yi [a], Rushi Vyas [b], Chunhee Cho [a], Chia-Hung Fang [a], James Cooper [b], Yang Wang [a]*,
Roberto T. Leon [c], and Manos M. Tentzeris [b]

[a] School of Civil and Environmental Eng., Georgia Inst. of Technology, Atlanta, GA 30332, USA
[b] School of Electrical and Computer Eng., Georgia Inst. of Technology, Atlanta, GA 30332, USA
[c] Department of Civil and Environmental Eng., Virginia Polytechnic Inst. and State Univ.,
Blacksburg, VA 24061, USA

ABSTRACT

For application in structural health monitoring, a folded patch antenna has been previously designed as a wireless sensor that monitors strain and crack in metallic structures. Resonance frequency of the RFID patch antenna is closely related with its dimension. To measure stress concentration in a base structure, the sensor is bonded to the structure like a traditional strain gage. When the antenna sensor is under strain/deformation together with the base structure, the antenna resonance frequency varies accordingly. The strain-related resonance frequency variation is wirelessly interrogated and recorded by a reader, and can be used to derive strain/deformation. Material properties of the antenna components can have significant effects on sensor performance. This paper investigates thermal effects through both numerical simulation and temperature chamber testing. When temperature fluctuates, previous sensor design (with a glass microfiber-reinforced PTFE substrate) shows relatively large variation in resonance frequency. To improve sensor performance, a new ceramic-filled PTFE substrate material is chosen for re-designing the antenna sensor. Temperature chamber experiments are also conducted to the sensor with new substrate material, and compared with previous design.

Keywords: passive wireless sensor; folded patch antenna; strain sensor; crack sensor; thermal effect; RFID

1. INTRODUCTION

Numerous studies have been conducted on the structural health monitoring (SHM) of deteriorating engineering structures, including those made of metallic materials [1]. In an SHM system, various types of sensors can be deployed, such as piezoelectric sensors/actuators [2], acoustic emission systems [3], fiber optic sensors [4], displacement sensors [5], accelerometers [6], etc. Although these sensing systems provide useful measurements, most current systems have limited applications due to their expensive or labor-intensive deployment. These limitations can be significant during large-scale/large-area deployment and continuous monitoring in the field.

To address these limitations, radiofrequency (RF) techniques have been exploited for wireless strain sensing in recent years. Since the electromagnetic resonance frequency of an antenna is related to antenna dimension [7], the resonance frequency changes when the antenna is subject to strain. This resonance frequency shift can be measured by an RF reader and used to derive strain/stress information. For example, a patch antenna sensor has been designed for wireless crack sensing, where the sensor requires light-switched circuitry for electromagnetic signal modulation [8].

In our previous study, a folded patch antenna was developed as a passive wireless antenna sensor for metallic structures [9]. The sensor has been tested for both strain sensing and crack sensing [10, 11]. Substrate material of the antenna sensor is Rogers RT/duroid® 5880, a glass microfiber-reinforced poly-tetra-fluoro-ethylene (PTFE) composite with dielectric constant ε_r of 2.2. The Rogers 5880 material is adopted due to its low dielectric attenuation, which improves the interrogation range of the antenna sensor. The sensor operation utilizes a backscattering mechanism, which refers to the deflection of electromagnetic wave from an object back to the source. A low-cost RFID chip is adopted to make the

---

* yang.wang@ce.gatech.edu; phone 1 404 894-1851; fax 1 404 894-2278; http://www.ce.gatech.edu/~ywang

sensor passive. The RFID chip obtains all its operation power from interrogation RF signal emitted by a wireless reader, eliminating the need for a battery or cabled power supply. Strain sensing performance of the RFID antenna sensor, such as sensing resolution and measurement limit, have been investigated through extensive tensile tests [11]. It is shown that the prototype antenna sensor can both measure small strain changes (<20 με) and perform well at large strains (> 10,000 με).

In this research, thermal effects on the antenna sensor performance are investigated. Numerical simulations to thermal deformation of the sensor are first performed, using a commercially available software package ANSYS. A temperature chamber test is then conducted for the prototype sensor. Chamber temperature is gradually changed from 122°F down to 32°F. At each temperature level, resonance frequency of the prototype sensor is wirelessly interrogated. Relationship between chamber temperature and antenna resonance frequency is investigated. To improve sensing performance under temperature fluctuation, an RFID antenna sensor with a new ceramic-filled PTFE substrate material, Rogers RT/duroid® 6202, is designed and fabricated. Temperature chamber test is conducted for the new sensor with Rogers 6202 substrate, and compared with the previous sensor with Rogers 5880 substrate. This paper is organized as follows. Section 2 introduces the strain sensing and wireless interrogation mechanism of the antenna sensor. Section 3 presents the simulation results for thermal deformation of the antenna sensor with Rogers 5880 substrate, and results of temperature chamber experiments. Section 4 describes a new sensor design with substrate material Rogers 6202, as well as temperature chamber test results.

2. WIRELESS STRAIN SENSING AND MEASUREMENT MECHANISM

Strain sensing mechanism of a prototype antenna sensor is first described in this section. Corresponding measurement technique for interrogation power threshold is then presented.

2.1 RFID antenna sensor design

Fig. 1 shows an illustration of the RFID antenna sensor. The sensor consists of three layers, i.e. top copper cladding and RFID chip, substrate as middle layer, and bottom copper cladding as ground plane. The substrate material adopted in this sensor is 31-mil-thick Rogers 5880, a glass microfiber-reinforced PTFE composite. Dimension of the top copper cladding is 2.15 in. × 1.97 in. To reduce overall size of the sensor, vias are used to connect the top copper cladding and bottom copper claddings, which effectively achieves antenna "folding." A low-cost off-the-shelf RFID chip from NXP Semiconductor (model number SL3ICS1002) is adopted, for harvesting energy from reader interrogation signal and responding to the reader. Top copper configuration is tuned to match the impedance of the RFID chip. Resonance frequency of this folded patch antenna can be estimated as:

$$f_{R0} = \frac{c}{4(L + L')\sqrt{\varepsilon_r}} \tag{1}$$

where f_{R0} is the antenna resonance frequency under zero strain, c is the speed of light, L is the physical length of the top copper cladding, L' is a small length compensation due to fringing effect, ε_r is the substrate dielectric constant. As shown
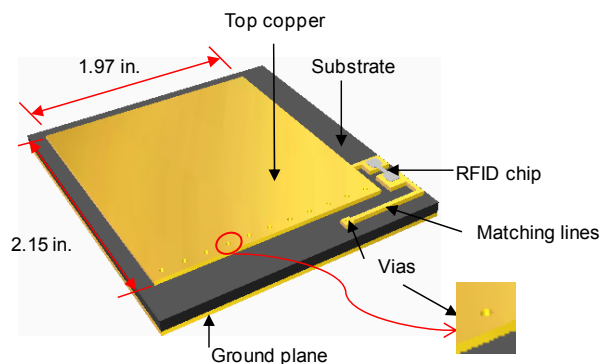

Fig. 1. RFID tag as an antenna sensor

in Eq. (1), antenna resonance frequency is related with physical length L. When the sensor is deformed, length L changes. With small strain ε (e.g. $< 10^{-3}$) occurring on the top copper cladding, the changed resonance frequency under strain, f_R, at room temperature is:

$$f_R = \frac{c}{4(L+L')(1+\varepsilon)\sqrt{\varepsilon_r}} \approx f_{R0}(1-\varepsilon) \tag{2}$$

The resonance frequency change, Δf, due to strain ε can be expressed as:

$$\Delta f = f_R - f_{R0} \approx -f_{R0}\varepsilon = S_\varepsilon\varepsilon \tag{3}$$

where S_ε ($= -f_{R0}$) is the theoretical strain sensitivity of the antenna sensor at room temperature. According to Eq. (3), the resonance frequency change has an approximately linear relationship with applied strain. The equation describes the basic strain sensing mechanism of the antenna sensor.

2.2 Strain measurement mechanism

To wirelessly interrogate resonance frequency change of the sensor under strain, a Tagformance Lite reader unit from Voyantic Ltd. is used. Fig. 2 shows a conceptual illustration of interrogation power threshold measurement provided by the reader. At each specific interrogation frequency, the reader changes transmission power level in order to identify an interrogation power threshold, which equals the power level that is just enough to activate the RFID chip and sensor response. The reader sweeps through a frequency range to find interrogation power threshold at different frequencies. As shown in Fig. 2, the interrogation power threshold versus frequency plot reaches minimum value at antenna resonance frequency, when minimum amount of interrogation power is required to activate the sensor response. After the antenna sensor is subject to strain, antenna length changes. According to Eq. (2), antenna resonance frequency changes correspondingly, which is also illustrated in Fig. 2. When strain ε is positive, resonance frequency f_R reduces. On the other hand, if strain ε is negative, resonance frequency f_R increases.

Strain sensing capability of the prototype antenna sensor has been validated by tensile tests. Experimental results reported in [11] show that the prototype antenna sensor can both measure small strain changes (<20 µε) and perform well at large strains (> 10,000 µε). As compared to the theoretical strain sensitivity S_ε described in Eq. (3), the experimental strain sensitivity measured from tensile testing, denoted as S_ε', is about -750 Hz/µε. This means 1 µε strain increment on the top copper cladding generates about 750Hz decrement in antenna resonance frequency. In addition, emulated crack tests show that the antenna sensor is capable of sensing milli-inch crack width and tracking its propagation [10].

3. THERMAL EFFECTS ON ANTENNA SENSOR WITH ROGERS 5880 SUBSTRATE

For field application on bridges or other civil structures, sensing stability against environmental temperature change is critical. In this section, simulation results on thermal deformation of the antenna sensor are first presented, followed by temperature chamber test results.
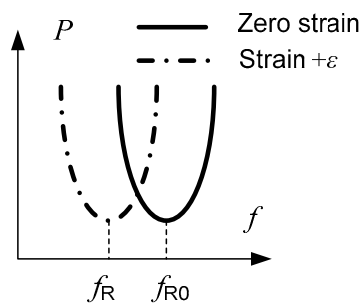

Fig. 2. Conceptual illustration of interrogation power threshold measurement

3.1 Effect of thermal deformation on antenna resonance frequency through simulation

Numerical simulations are first performed to study sensor deformation due to temperature increase, when the antenna sensor is bonded to an unconstrained aluminum specimen. Table 1 shows key material properties used in the simulation. Materials in the sensor include Rogers 5880 substrate and copper claddings. All three materials listed in Table 1 have different thermal expansion coefficients (T.E.C.). In particular, the substrate material Rogers 5880 is inhomogeneous, with different T.E.C. along three directions. In order to evaluate complicated strain distributions due to temperature fluctuation, a thermal-mechanical coupled simulation is conducted using ANSYS software.

Most of the dimension and material properties in Table 1 reflect the actual scenario to be tested in a temperature chamber. The main difference is that aluminum specimen length is slightly reduced in simulation to save computing effort. For simplicity, bonding glue between the substrate and aluminum specimen is omitted in simulation, i.e. top surface of aluminum specimen and bottom surface of the substrate share same finite element nodes between them. The matching line, vias, and bottom copper cladding are regarded to have minimal effect on mechanical analysis, and thus, not considered in this simulation. Exploiting the symmetry of the problem, only one quarter of the structure (dimensions listed in Table 1) is built in ANSYS. Fig. 3 illustrates the ANSYS meshing of the quarter model. A quarter of the antenna sensor is located in Area 1 (lower-left of the figure). Under the antenna sensor, a quarter of the aluminum specimen occupies all areas in the figure. Symmetric boundary condition is assigned to the left and lower sides of the model. Free boundary condition is assigned to the upper and right side, to allow unconstrained stress-free thermal deformation.

The copper cladding, sensor substrate, and aluminum specimen in Area 1 are modeled as ANSYS SOLID45 elements at high resolution. The aluminum specimen in Area 3 is modeled as SOLID45 elements at relative low resolution, to reduce computing effort. Since SOLID95 type is a 20-node element suitable for transiting between areas with different meshing resolutions, it is used to model elements in Area 2 that is between Areas 1 and 3. Along thickness direction of the sensor, one layer of elements is assigned for the copper claddings, and five layers of elements are assigned for the substrate. For the aluminum specimen, Area 1 has four layers along the thickness direction, Area 3 has two layers, and

Table 1. Key properties of the material in the test specimen

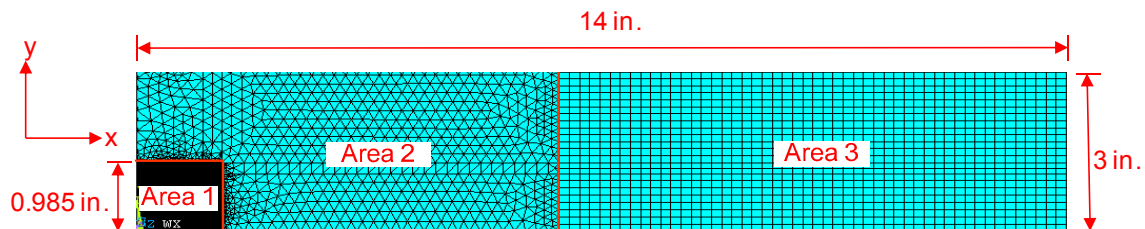|		Rogers 5880 (Glass microfiber reinforced PTFE composite)	Copper cladding	6061 aluminum specimen
Coefficient of thermal expansion (ppm/ºF)	x	17	9	13
	y	27		
	z	132		
Dimension (in.)		2.72 × 2.4 × 0.031	2.15 × 1.97 × 0.0007	28 × 6 × 0.125
Young's modulus (ksi)		156	17,000	10,000
Poisson's ratio		0.33	0.33	0.3

Fig. 3. Meshing of the quarter ANSYS model for mechanical simulation (Area 1: a quarter of the RFID sensor; Areas 1, 2, and 3 combined: a quarter of the aluminum specimen).
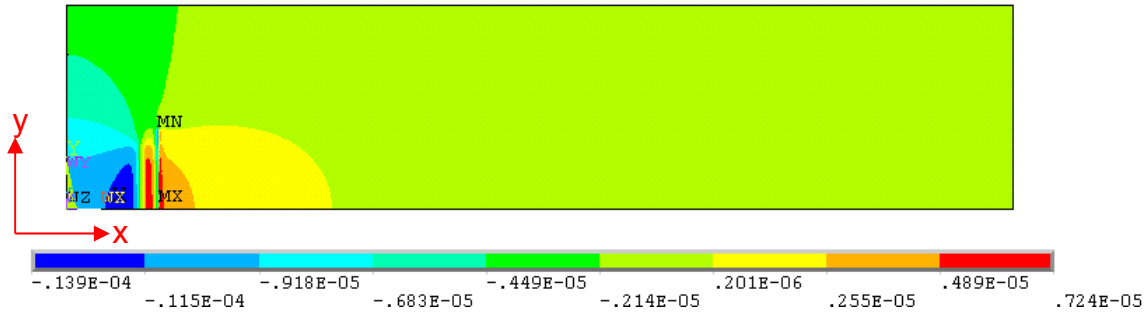
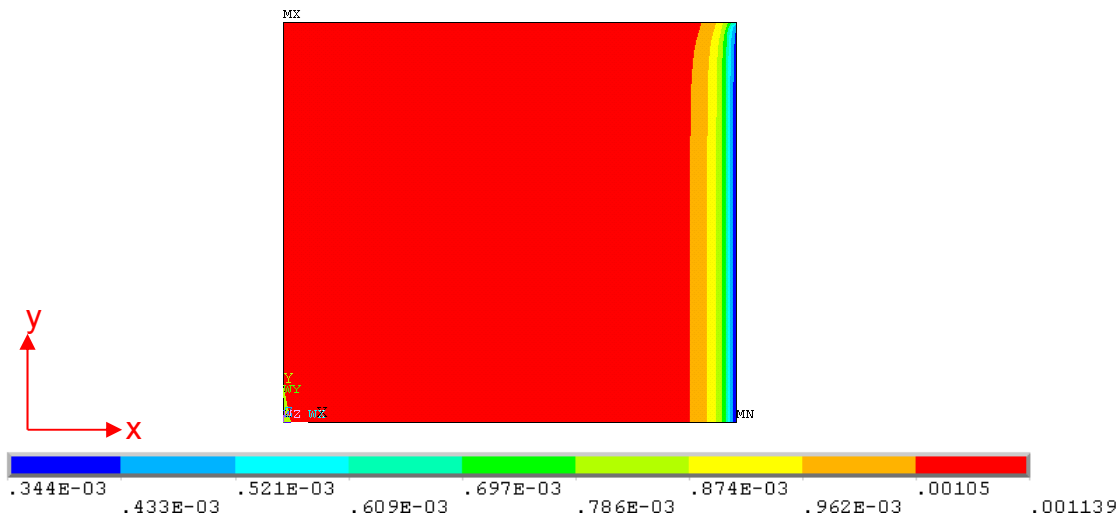Fig. 4. X-direction strain on aluminum specimen

Fig. 5. X-direction strain on top copper cladding

Area 2 is automatically meshed when transiting from two to four layers.

A uniform temperature increase of 90 °F is applied to the ANSYS model. Fig. 4 shows x-direction strain on the top surface of aluminum specimen. Fairly uniform strain distribution is observed at the right end of the specimen. Fig. 5 shows strain distribution on the top surface of copper cladding. Strain on the copper is also uniformly distributed, except for the right edge. Average strain level on the copper cladding is approximately 1,100με. The strain sensitivity in X-direction due to temperature change, α, is calculated as:

$$\alpha = \frac{1,100\mu\varepsilon}{90°F} = 12.2\mu\varepsilon/°F \tag{4}$$

Since the measured resonance frequency change due to strain is $S_\varepsilon' = -750$ Hz/ με, resonance frequency change of the sensor due to temperature change, S_T, can be calculated as:

$$S_T = S_\varepsilon' \cdot \alpha = -750 \times 12.2 = -9.15 \text{kHz}/°F \tag{5}$$

To verify the resonance frequency versus temperature change, temperature chamber test is conducted.

3.2 Temperature chamber test evaluating thermal effects to antenna resonance frequency

Temperature chamber test is conducted to study the antenna resonance frequency change caused by temperature fluctuation. Fig. 6 shows the test setup. An antenna sensor together with aluminum specimen is placed in the chamber. The Tagformance reader (described in Section 2.2) is used for wireless interrogation. Reader antenna is placed 12 in.

away from the sensor. Because all walls, ceiling, and floor of the temperature chamber are furnished with metal surfaces, large amount of electromagnetic wave reflection to reader interrogation signal is expected. To reduce the effect of reflection on wireless interrogation, four pieces of radiation-absorbent foams are places around the test specimen and reader antenna. To keep track of temperature fluctuations in the chamber, five thermometers are placed around the foams, as shown in Fig. 6(a).

Fig. 7 shows the temperature steps of the test. The chamber temperature is first increased to 122°F within 30 minutes, and held at 122°F for 1 hour to achieve uniformity and stability. During the test, the chamber temperature is reduced by 9°F after every 30 minutes, to the final level at 32°F. Interrogation power threshold measurement is conducted at each temperature level, before temperature reduction to next level. To reduce environmental noise, five frequency sweeps are performed in the measurement. The average interrogation power threshold at different temperature levels are plotted in Fig. 8(a). For clarity, only four temperature levels are shown. The temperature listed in the legend of Fig. 8(a) is the average reading among five thermometers around the specimen. Compared with target temperature levels shown in Fig. 7, actual measured temperatures are slightly lower. The discrepancy is because control thermostat is located close to an inlet opening on the wall, where temperature is higher than the center of the chamber. Resonance frequency of the

(a) Front view (test specimen is enclosed by foams)   (b) Top view
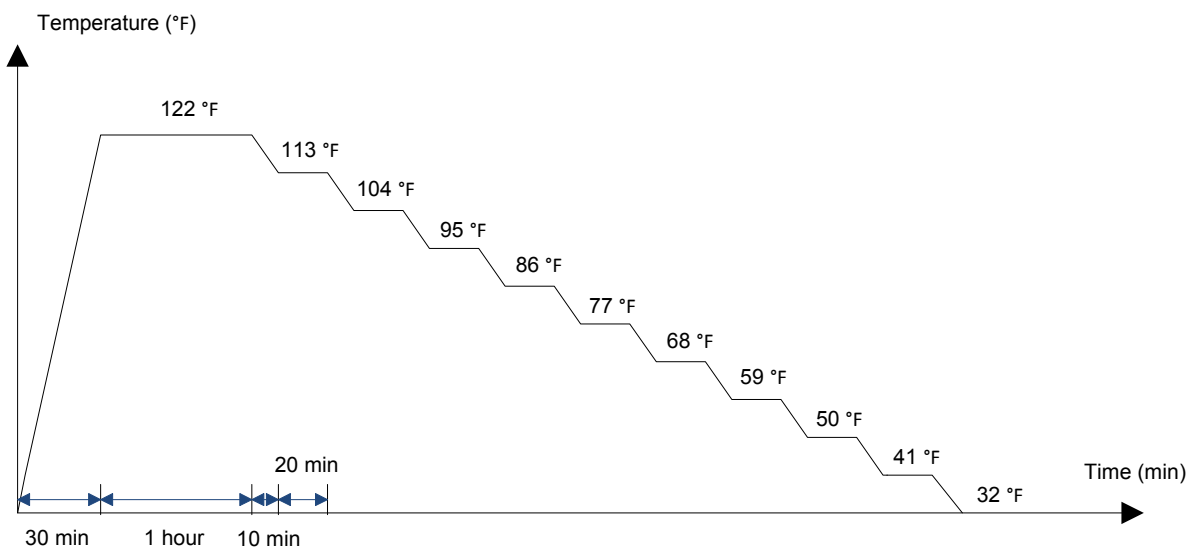Fig. 6. Experimental setup for temperature chamber test

Fig. 7. Target temperature levels during temperature chamber test

(a) Average interrogation power (in dBm)　　(b) Resonance frequency change during temperature
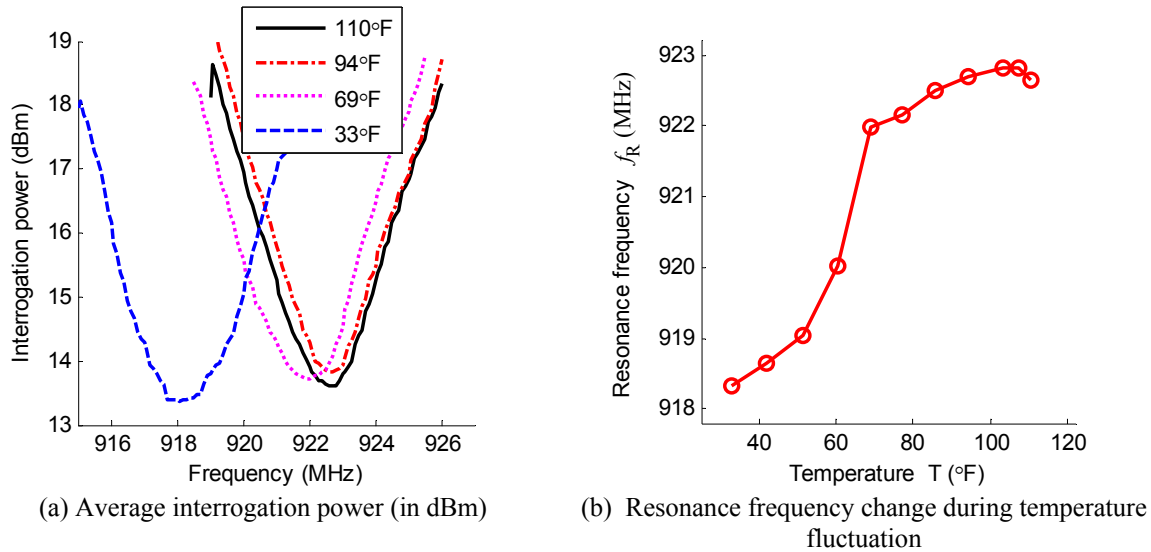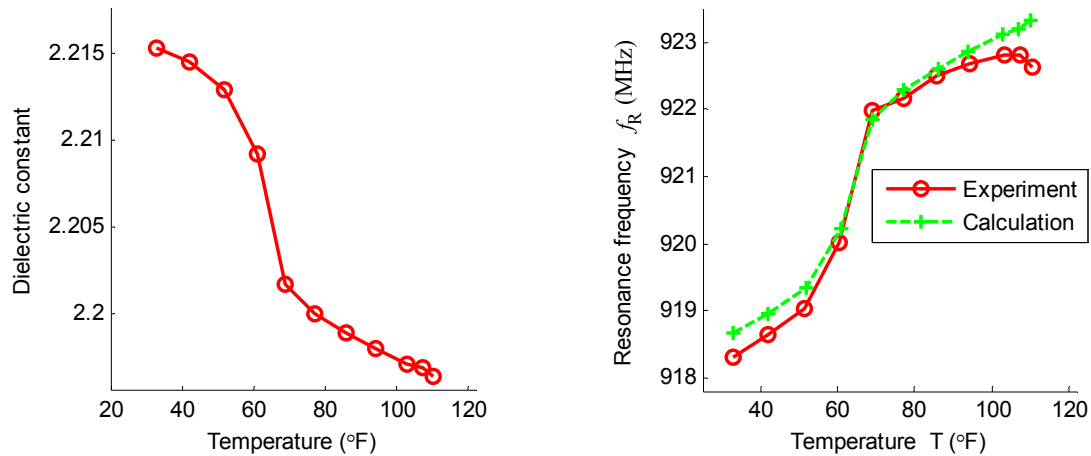fluctuation

Fig. 8. Temperature chamber test results (antenna sensor with Rogers 5880 substrate)

antenna sensor decreases as the chamber temperature reduces. Since the valley area of each curve is not smooth, a fourth order fitting is applied to curves shown in Fig. 8(a). Resonance frequency at each temperature level is thus determined by peak picking of each fitted curve, and shown in Fig. 8(b). A total of about 5 MHz resonance frequency decrease is observed when the chamber temperature reduces from 110°F down to 32°F. As estimated in Section 3.1, the resonance frequency change of the sensor due to thermal expansions is only −9.15 kHz/°F. If thermal expansion were the only cause for resonance frequency change, the resonance should have increased by 0.714 MHz when temperature reduces from 110°F down to 32°F. Because a 5 MHz decrease in observed instead during the experiment, it is concluded that thermal deformation is not the main reason for resonance frequency change when temperature fluctuates.

In fact, it is identified that most of the resonance frequency change is caused by substrate dielectric constant change due to temperature fluctuation. Fig. 9(a) shows Rogers 5880 dielectric constant change due to temperature fluctuation [12]. According to Eq. (1), decrease in the dielectric constant causes increase in resonance frequency. Combining data in Fig. 9(a) and thermal expansion effect described in Section 3.1, the resonance frequency at different temperatures can be calculated. Define the zero-strain resonance frequency f_{R0} (see Eq. (1)) at room temperature 73°F as reference state of the sensor. The resonance frequency at another temperature T is calculated as:

$$
\begin{aligned}
f_R^T &= f_R \sqrt{\frac{\varepsilon_r}{\varepsilon_r^T}} \\
&= (f_{R0} + \Delta f_R)\sqrt{\frac{\varepsilon_r}{\varepsilon_r^T}} \\
&\approx f_{R0}\sqrt{\frac{\varepsilon_r}{\varepsilon_r^T}} + S_T \cdot \Delta T \sqrt{\frac{\varepsilon_r}{\varepsilon_r^T}}
\end{aligned}
\tag{6}
$$

where ε_r and ε_r^T is the substrate dielectric constant at reference temperature 73°F and another temperature T, respectively; ΔT is the temperature difference from 73°F reference; $\Delta f_R (\approx S_T \cdot \Delta T)$ is the resonance frequency change due to thermal expansion. Fig. 9(b) overlays the calculation results with experimental results, showing a close match. It is therefore concluded that resonance frequency change during temperature fluctuation is mainly caused by change in substrate dielectric constant.

(a) Dielectric constant change during temperature fluctuation [12]

(b) Resonance frequency change during temperature fluctuation

Fig. 9. Effect of dielectric constant change during temperature fluctuation (Rogers 5880 substrate)

4. ANTENNA SENSOR DESIGN AND TEST WITH ROGERS 6202 SUBSTRATE

To improve sensor reliability when temperature fluctuates, a new substrate material has been identified. The material has more stable dielectric constant under temperature fluctuation. This section describes the effort to re-design and test an antenna sensor with the new substrate material.

A new substrate material, Rogers 6202 (ceramic-filled PTFE composite) is chosen for a redesign of the antenna sensor. Table 2 lists key properties of substrate material Rogers 6202, as compared with Rogers 5880. The coefficients of thermal expansion of Rogers 6202 are reduced by half in x and y direction, and reduced by 87% in z direction. With less thermal deformation under temperature fluctuation, more stable resonance frequency is also expected when temperature fluctuates.

More importantly, dielectric constant of Rogers 6202 at different temperatures is plotted in Fig. 10. Much smaller dielectric constant change is observed, as compared with Rogers 5880 shown in Fig. 9(a). With smaller dielectric constant change and less thermal deformation under temperature fluctuation, more stable resonance frequency is expected when temperature fluctuates. The new sensor configuration with Rogers 6202 substrate is shown in Fig. 11. Since the dielectric constant magnitude of Roger 6202 is larger than Roger 5880, total copper size of the sensor decreases from 2.15 in. × 1.97 in. to 1.91 in. × 1.73 in. Matching lines are re-tuned to match the impedance of the RFID chip.

Table 2 Key properties comparison of Rogers 5880 and Rogers 6202

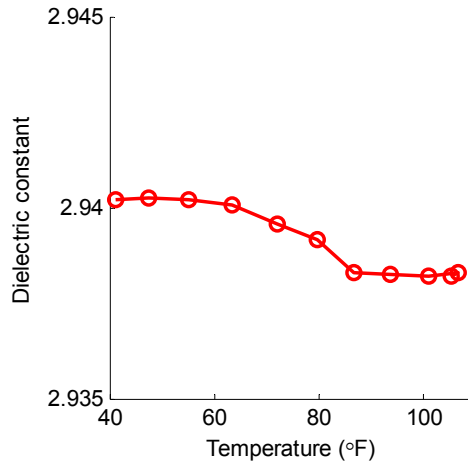|		Rogers 5880	Rogers 6202
Material type		Glass microfiber reinforced PTFE composite	Ceramic filled PTFE composite
Coefficient of thermal expansion (ppm/ºF)	x	17	8
	y	27	8
	z	132	17
Dielectric constant (ε_r) at 73 ºF		2.2	2.94

Fig. 10. Dielectric constant change of Rogers 6202 due to temperature fluctuation (provided by manufacturer)

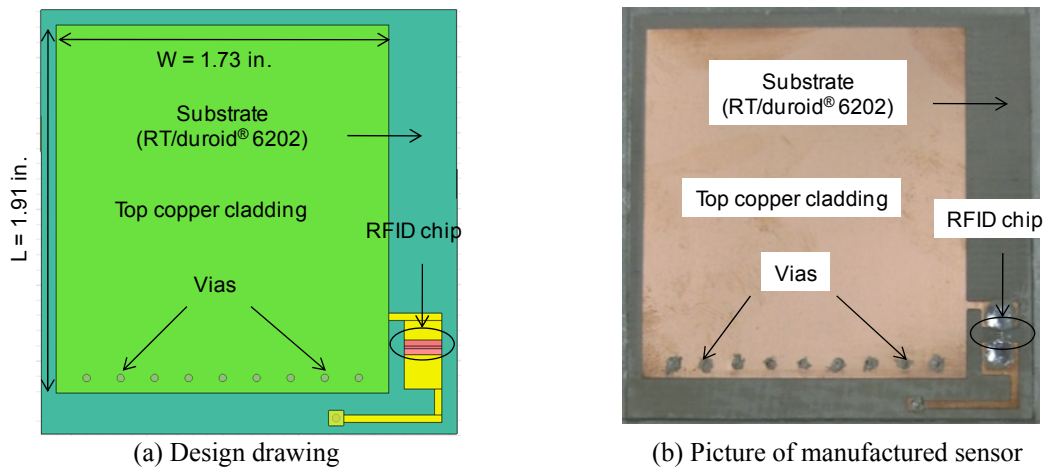(a) Design drawing   (b) Picture of manufactured sensor

Fig. 11. Antenna sensor with Rogers 6202 substrate material

After the new sensor with Rogers 6202 substrate is fabricated, temperature chamber test is conducted. The experimental results are shown in Fig. 12. Average interrogation power threshold at different temperatures is plotted in Fig. 12(a). For clarity, only four temperature levels are shown. The extracted resonance frequencies at different temperatures are plotted in Fig. 12(b). Overall, the resonance frequency change is only about 0.2 MHz when temperature changes from 41 °F to 105 °F. Compared with previous sensor design with Rogers 5880 substrate, it is obvious that Rogers 6202 provides much better temperature stability in resonance frequency. More tensile experiments are required to explore the thermal expansion effects.

5. SUMMARY AND DISCUSSION

This paper discusses thermal effects on an antenna sensor recently developed for wireless strain and crack sensing. Thermal expansion and dielectric constant change of the previous sensor design (with Rogers 5880 substrate) are studied under temperature fluctuation. Temperature chamber test is conducted. It shows that the sensor has a relatively large resonance frequency change due to its large dielectric constant variation under temperature fluctuation.

To improve sensor performance during temperature fluctuation, a new antenna sensor is designed using Rogers 6202 substrate whose dielectric constant is more steady when temperature fluctuates. Temperature chamber test shows the
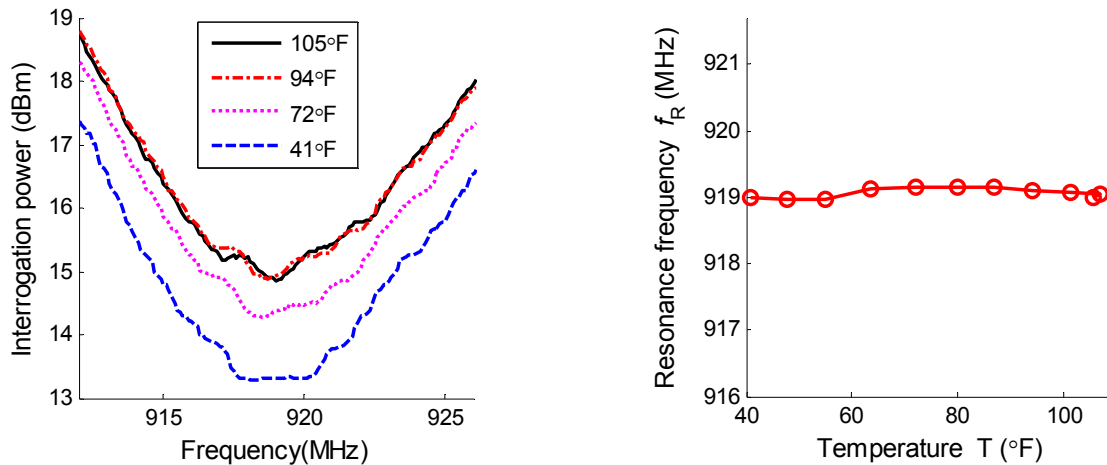
(a) Average interrogation power threshold (in dBm)   (b) Resonance frequency change during temperature fluctuation
Fig. 12. Temperature chamber test results (antenna sensor with Rogers 6202 substrate)

sensor with Rogers 6202 substrate has a more consistent resonance frequency under temperature fluctuation. In future study, exhaustive tensile and crack tests will be performed in order to characterize the performance of the new antenna sensor with Rogers 6202 substrate.

ACKNOWLEDGEMENT

REFERENCES

[1] Chang, P.C., Flatau, A. and Liu, S.C., "Review paper: health monitoring of civil infrastructure," *Struct. Health Monit.*, 2(3), 257-267 (2003).
[2] Ihn, J.-B. and Chang, F.-K., "Detection and monitoring of hidden fatigue crack growth using a built-in piezoelectric sensor/actuator network: I. Diagnositcs," *Smart. Mater. Struct.*, 13, 609-620 (2004).
[3] Roberts, T.M. and Talebzadeh, M., "Acoustic emission monitoring of fatigue crack propagation," *J. Constr. Steel Res.*, 59, 695-712 (2003).
[4] Li, H., Li, D. and Song, G., "Recent applications of fiber optic sensor to health monitoring in civil engineering," *Eng. Struct.*, 26, 1647-1657 (2004).
[5] Brownjohn, J.M.W., "Structural health monitoring of civil infrastructure," *Phil. Trans. R. Soc. A*, 365, 589-622 (2007).
[6] Barke, D. and Chiu, W.K., "Structural health monitoring in the railway industry: a review," *Smart. Mater. Struct.*, 4(1), 81-94 (2005).
[7] Balanis, C.A., [Antenna Theory: Analysis and Design], John Wiley & Sons: New York (1997).
[8] Tata, U., Huang, H., Carter, R.L. and Chiao, J.C., "Exploiting a patch antenna for strain measurements," *Meas. Sci. Technol.*, 20(1), 015201 (2009).
[9] Yi, X., Wu, T., Wang, Y., Leon, R.T., Tentzeris, M.M. and Lantz, G., "Passive wireless smart-skin sensor using RFID-based folded patch antennas," *Int. J. Smart Nano Mater*, 2(1), 22-38 (2011).

[10] Yi, X., Cooper, J., Wang, Y., Tentzeris, M.M. and Leon, R.T., "Wireless crack sensing using an RFID-based folded patch antenna," Proceeding of the 6th International Conference on Bridge Maintenance, Safety and Management, Lake Como, Italy (2012).

[11] Yi, X., Wu, T., Lantz, G., Cooper, J., Cho, C., Wang, Y., Tentzeris, M.M. and Leon, R.T., "Sensing resolution and measurement range of a passive wireless strain sensor," Proceedings of the 8th International Workshop on Structural Health Monitoring, Stanford, CA, USA (2011).

[12] Rogers Corporation, "Properties of low dielectric constant laminates," EMPFasis, March 2010, (2010).